Model Predictive Control with a Cascaded Hammerstein Neural Network of a Wind Turbine Providing Frequency Containment Reserve

Nezmin Kayedpour, *Student Member, IEEE,* Arash E. Samani, *Student Member, IEEE,* Jeroen D. M. De Kooning, *Senior Member, IEEE,* Lieven Vandevelde, *Senior Member, IEEE,* Guillaume Crevecoeur, *Senior Member, IEEE*

***Abstract*—This article presents an application of neural network-based Model Predictive Control (MPC) to improve the wind turbine control system's performance in providing frequency control ancillary services to the grid. A closed-loop Hammerstein structure is used to approximate the behavior of a 5MW floating offshore wind turbine with a Permanent Magnet Synchronous Generator (PMSG). The multilayer perceptron neural networks estimate the aerodynamic behavior of the nonlinear steady-state part, and the linear AutoRegressive with Exogenous input (ARX) is applied to identify the linear time-invariant dynamic part. Using the specific structure of the Cascade Hammerstein design simplifies the online linearization at each operating point. The proposed algorithm evades the necessity of nonlinear optimization and uses quadratic programming to obtain control actions. Eventually, the proposed control design provides a fast and stable response to the grid frequency variations with optimal pitch and torque cooperation. The performance of the MPC is compared with the gain-scheduled proportional-integral (PI) controller. Results demonstrate the effectiveness of the designed control system in providing Frequency Containment Reserve (FCR) and frequency regulation in the future of power systems.**

***Index Terms*—Wind turbine, Neural networks, Model approximation, Hammerstein structure, Predictive controller, Frequency containment reserve.**

NOMENCLATURE

Δf	Incremental change in frequency
ΔP	Incremental change in power
Δu	Increments vector for manipulated variables
Ω_r	Rotor speed
θ_c	Collective pitch angle
φ	Nonlinear transfer function
a, b	Parameters of linearization
C_F	Thrust coefficient
C_p	Power coefficient
C_T	Torque coefficient
D	Droop control coefficient
f_{actual}	Actual grid frequency
f_{ref}	Reference frequency (50 Hz)
F_a	Rotor thrust
G	Dynamic matrix
$J(K)$	Cost function
K	Sample instance
k^s	Number of hidden nodes
N	Prediction horizon
n_a, n_b	Constant defining the order of the dynamic model
n_k	Constant defining the delay in the dynamic model
n_r	Number of outputs of the nonlinear steady-state part
N_u	Control horizon
n_u	Number of manipulated variables
n_x	Number of inputs of the nonlinear steady-state part
P_a, Pg	Aerodynamic power, generator power
P_e	Electrical power
P_e^{dl}	Deloaded power
P_e^{ref}	Operating power reference
R	Blade radius
S_p	Step response coefficients
T_a, T_g	Rotor torque, generator torque
$V(K)$	Vector of auxiliary variables
v_w	Wind speed
$w_{i,j}^{1,r}$	Weights of first layer of the neural network
$w_i^{2,r}$	Weights of second layer of the neural network
x_r	Outputs of nonlinear steady-state part
z_i^r	Sum of input signals connected to i^{th} hidden node

N. Kayedpour, A. E. Samani, L.Vandevelde and G. Crevecoeur are with, the Department of Electromechanical Systems and Metal Engineering, Ghent University and FlandersMake@UGent—corelab EEDT-DC, Gent, Belgium (e-mail: nezmin.kayedpour@ugent.be; ebnealisamani.arash@ugent.be; lieven.vandevelde@ugent.be; guillaume.crevecoeur@ugent.be).

J D. M. De Kooning is with, the Department of Electromechanical Systems and Metal Engineering, Ghent University and FlandersMake@UGent—corelab EEDT-MP, Gent, Belgium (email: jeroen.dekooning@ugent.be).

I. INTRODUCTION

MODERN wind turbines are designed to operate over a wide range of wind speeds to make wind energy more cost-effective. However, these wind energy sources generate fluctuating power due to their dependency on the intermittent and variable wind. This issue hinders retaining adequate levels of reliability and stability of the power grid, and the balance of electricity supply-demand. Hence posing significant challenges to the integration of wind energy into the power system [1].

While offshore wind farms are growing in size, the need arises for these sources to take part in grid balancing and stabilization, e.g., by providing ancillary services [2].The Frequency Containment Reserve (FCR), formerly known as the primary frequency reserve, is used to regulate the frequency deviation caused by the sudden changes in the generation or load. Offshore wind turbines offer the potential for providing FCR since the wind flow is less variable compared to inland wind farms where obstacles may divert the wind flow [3], and specifically in above-rated wind speeds. However, the wind turbine control system's capability in providing FCR is challenged by the frequent changes in operating points and

delivering a fast optimal response in the presence of varying wind speed. These challenges need to be addressed in order to increase the further share of wind power in the future power system [4].

Over the past decades, the wind turbine control system's primary goal was rotor speed regulation and maximum power point tracking with a Proportional-Integral (PI) design. However, current wind turbines are needed to satisfy the grid code technical requirements and additional operating conditions demanded by transmission system operators [5]–[7]. Some studies suggest that torque control and pitch control can act as frequency regulation schemes [8], [9]. One approach is that the wind turbine operates in the MPPT mode, and the power response to frequency variations on a short time scale can be answered by the inertia characteristics. However, this strategy may cause system instability due to the rapid variations in the rotational speed of the wind turbine [10]–[13]. Another scheme is that the wind turbine does not operate in MPPT mode, but instead operates at the suboptimal operating limit by under-speeding or over-speeding control methods to obtain a power reserve for frequency regulation [14], [15]. As a counterpoint, providing power reserve with de-loaded wind turbines in below-rated wind speed result in a reduced energy yield. On the other hand, the frequency control scheme, which only relies on the pitch control system, does not necessarily regulate the frequency variations to a full extent due to the typical delay of the pitch actuator [10]. Thus, the need arises for an advanced control design with varying control policies to cope with the system's complexity, its physical constraints, and the intermittent nature of wind, which enables the wind turbine to provide FCR by taking advantage of the optimal interaction between pitch and torque control.

In recent years, advanced optimal control methods such as Linear Quadratic Gaussian (LQG), fuzzy logic, and H∞ have been applied in wind turbine control systems concerning the power grid integration [16]–[19]. Despite the robust behavior of these controllers in maximizing energy conversion, frequency regulation, or even structural load mitigation, the control performance can still be improved further, which can be attributed to the intrinsic nonlinearity of the system and/or the difficulties to incorporate physical constraints.Model-based Predictive Control (MPC) is becoming increasingly popular in wind energy applications. It possesses the inherent ability to deal with multi-input multi-output systems and constraints imposed on manipulated variables [20]. Additionally, MPC can be made robust to plant uncertainties [10] and measurement uncertainties [21]. Finally, MPC has the ability to incorporate wind speed estimation [21].

Linear MPC based on a linearized wind turbine model has been widely used because it requires less programming and computational power than scheduled MPC or nonlinear adaptive MPC. For instance, [20] claims that the implementation of a linear MPC algorithm, based on linearization along with a single operating point, can achieve a suitable performance in the entire range of wind turbine operation, as long as the underlying design is robustly made. However, the parametric uncertainties in the model and the presence of disturbances can significantly affect the underlying robustness and may degrade MPC's performance in the whole operating range [22], [23].

Scheduled MPC can realize significant load mitigation and reliable power reference tracking throughout the entire operating region [24]. Soliman et al. proposed in [25] an MPC technique for controlling a variable-speed variable-pitch wind turbine that switches between multiple linear models that each are valid at different operating points. However, when designing scheduled MPC, varying operating conditions impose difficulties on a smooth switching performance, especially in the transition between partial load region and full load region where the control variable changes between torque and pitch. In [26] Ebadollahi et al. introduce a new soft-switching multiple MPC based on the gap metric and Kalman filter estimator for reduction of torque oscillation but only in the partial load region. Moreover, nonlinear MPC applications with a nonlinear optimization algorithm have become increasingly performant but are still computationally demanding. In their implementation, control actions need to be taken within a bounded time that are not always met [27]. Artificial Neural Networks offer the advantage of learning from sensory data to optimize the wind turbine's performance in stochastic conditions and furthermore fasten computing the control actions [28], [29].

The purpose of this study is to improve the capability of an offshore floating wind turbine in providing FCR, based on cooperation between the torque and the pitch controller, by taking advantage of data-driven techniques and optimal predictive control. The primary reserve is achieved through a balance type control, where an absolute power set-point is chosen below the available power [6], [7], [30]. In this case, the turbine will produce maximum output power up to the desired power set-point and responds to the grid frequency changes by tracking the reference power through optimal performance of pitch and torque.

To carry out the proposed approach, a 5MW offshore floating wind turbine is firstly simulated by using the Fatigue Aerodynamic Structure and Turbulence (FAST) software provided by the National Renewable Energy Laboratory (NREL) [31], [32]. Next, the nonlinear approximations and linear modeling have been carried out based on the simulations' obtained datasets in a turbulent wind condition, which can strongly detail the wind turbine nonlinear dynamics. Subsequently, a neural network-based MPC algorithm, proposed in [33], is implemented, and its control performance in providing FCR is evaluated. The proposed derivative-free optimization method uses neural networks to relax the need for an analytical model of a large-sized wind turbine, which would require the high numerical effort of computational fluid dynamics. [34].

To circumvent using nonlinear optimization methods, we have applied a linearization, based on Taylor series expansion, around the operating point such that a quadratic optimization problem can be formulated. For this purpose, the AutoRegressive with Exogenous input (ARX) model is used as a linear function of the calculated future input sequence. The calculated control inputs should satisfy the physical limitations of pitch and torque. Therefore, the determined vectors of constraints are projected onto the set of feasible solutions. Finally, a frequency profile is used to test the proposed design's

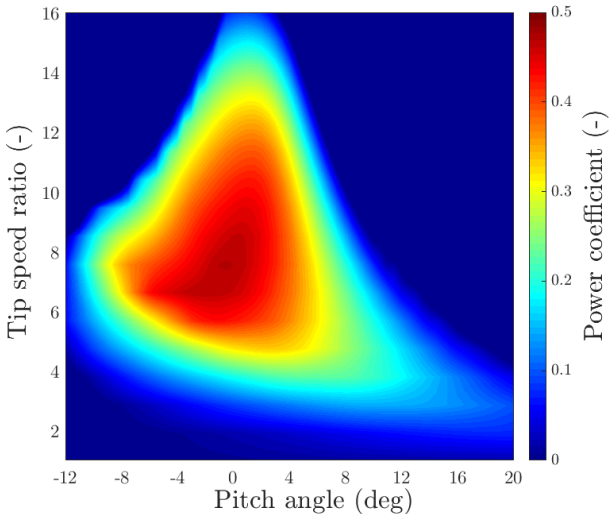


Figure 1: NREL 5-MW offshore wind turbine power coefficient as a function of tip speed ratio and pitch angle.

effectiveness in power reference tracking through a comparative study. The simulation results confirmed that the proposed control approach has the ability to provide transient and steady-state power reference tracking and effectively improve the stabilization of the active power control with an optimal and secure operation of the wind turbine.

The article is organized as follows: The 5MW wind turbine dynamic model and the baseline control structure are discussed in section II. Section III introduces the data-driven model approximation based on the cascade Hammerstein structure using multi-layer perceptron (MLP) neural networks and linear ARX underpinning the proposed MPC structure. Section IV formulates the proposed control strategy. The controller performance assessment and clarification are given in section V. Discussion and conclusions are drawn in section VI.

II. WIND TURBINE DESIGN

A. Wind turbine dynamic model

The wind energy conversion system includes wind turbine dynamics and a PMSG with a power electronic converter that subsequently converts the mechanical energy into electrical power. The aerodynamic power of the turbine rotor P_a is a function of power coefficient and wind speed.

$$P_a = \frac{1}{2}\rho\pi R^2 v_w^3 C_p(\lambda, \theta_c) \tag{1}$$

where R, v_w, and ρ are the blade radius, wind speed, and air density, respectively. The power coefficient $C_p(\lambda, \theta_c)$ is a function of tip speed ratio and collective pitch angle θ_c. The tip speed ratio λ is defined as the ratio of rotor speed Ω_r at the tip of blades to the wind speed $\lambda = R\Omega_r/v_w$. Figure 1 shows the power coefficient of the NREL 5MW offshore wind turbine as a function of tip speed ratio and pitch angle. The maximum power coefficient of 0.48 is achieved at the pitch angle 0 and a tip speed ratio of 7.5.

The NREL 5-MW offshore wind turbine with given parameters in Table I, can be controlled by means of three kinds of manipulative inputs, i.e., nacelle yaw angle, pitch angle, and generator torque T_g. In this work, it is assumed that there is no changing direction in wind speed; hence the nacelle yaw angle actuator is disabled, and both torque and pitch control systems with the baseline PI controller are used to control the aerodynamic power capture and rotational speed. The dynamic equation of the wind turbine is described by

$$T_a - T_g = F\Omega_r + J\frac{d\Omega_r}{dt} \tag{2}$$

with J being the moment of inertia, F is the viscous friction coefficient and $T_a = \frac{P_a}{\Omega_r}$ is the mechanical torque. Furthermore, the electric output power of the generator is defined as follows

$$P_g = \eta_g T_g \Omega_r \tag{3}$$

where, η_g is the generator efficiency. The FAST 5-MW baseline wind turbine model is coupled to a generator and converter model implemented in Matlab/Simulink. The generator is a direct-drive PMSG, which is modeled with an equivalent scheme in the rotating reference frame, as presented in [35]. The efficiency curve is included in the model as a function of different operating points. This model offers a realistic representation of the dynamics and losses of the machine since it includes machine inductances, armature reaction effect, stator copper losses, and iron core losses. The generator control is a field orientation control, which offers direct control of the generator torque by regulating the q-axis current to a set-point value while keeping the d-axis current at zero. The power-electronic converter is not modeled up to the switching level, but an efficiency curve is included. The efficiency curve is obtained from a separate Simulink model, including both conduction and switching losses, in which the converter was modeled up to the switching level [36].

Table I: NREL 5 MW wind turbine parameters

Parameters	Values
Rated Power	5 MW
Rotor Orientation	Upwind
Configuration	3 Blades
Control	Variable Speed, Collective Pitch
Cut-In, Rated, Cut-Out Wind Speed	3 m/s, 11.4 m/s, 25 m/s
Cut-In, Rated Rotor Speed	6.9 rpm, 12.1 rpm
Rated Tip Speed	80 m/s

B. The baseline control design

The pitch and torque baseline controllers are designed to work under specific wind conditions. The operating mode depends on the wind speed and can be divided into four operating regions [31]. In the first two regions where the wind speed is below the rated value, the pitch angle is kept in an optimal position to extract the maximum aerodynamic power while the generator torque varies proportionally to the square of the generator speed as follows

$$T_{\mathrm{g-ref}}(t) = K_{\mathrm{opt}}\Omega_r^2 \tag{4}$$

where K_{opt} is calculated by the maximum power coefficient $C_{\mathrm{p-Max}}$ curve and the optimal tip speed ratio.

$$K_{\mathrm{opt}} = \frac{1}{2}\rho\pi R^5 \frac{\mathrm{C_{p-Max}}}{\lambda_{\mathrm{opt}}^3} \tag{5}$$

In region two, a cascaded control system is designed to control the rotational speed by regulating the generator torque. The outer PI controller is the (slow) power controller providing the reference signal to the inner current controller. The fast inner PI control loop regulates the generator current by rectifier control. A pre-defined look-up table determines the reference signal of the cascaded control system. The look-up table is generated from the power-speed curves obtained through simulations. The third region, which is known as the transition mode between the second and fourth regions, can be considered as an extension of the second. In this region, the main concern is to regulate generator speed at rated power by using the pitch control. In the fourth region, where the wind speed is above the rated value, the main control objective is to regulate power capture at the rated power by means of pitch control. In this region, the constant PI gains are not adequate for effective speed control due to aerodynamic power's sensitivity to the blade pitch angle, which considerably varies during the active power control [32]. However, since the relation between pitch sensitivity and blade pitch angle is nearly linear, the gain scheduling is implemented based on the gain correction factor determined from pitch sensitivity analysis. The gain-scheduled proportional-integral (PI) pitch controller is developed at each operating point to cope with this nonlinear aerodynamic sensitivity. The blade-pitch sensitivity is calculated for the NREL 5-MW model by performing a linearization analysis in FAST.

Furthermore, to be able to provide FCR, a supplementary control loop is required to control the active power output responding to grid frequency changes. In [7], three de-loading modes, based on the torque-speed tracking controller, are presented. In this study, the first mode is used, which reserves a constant percentage of rated power, and enables the wind turbine to track the power command based on absolute de-loaded power when the wind speed is above the rated value. In this case, the turbine will produce maximum output power up to the desired power set-point. There would be no available reserve margin when the wind speed is below the rated value, and the wind turbine only operates in MPPT mode.

C. Wind estimation

In this article, the proposed MPC strategy uses the preview of the wind speed over the prediction horizon. The rotor inflow wind speed is simulated by TurbSim [37]. In reality, LIDAR systems are capable of scanning the incoming raw wind data and extract the wind estimation [38]. We used a data-driven approach for carrying out the short-term prediction of wind speed with data collected at 10-millisecond sample time. A Group Method of Data Handling (GMDH) is used as a semi-supervised deep learning tool that automatically self-organizes the predictive distribution of variables. GMDH is a nonlinear regression method capable of driving the best polynomial network structure to predict future values from the historical time-series [39].

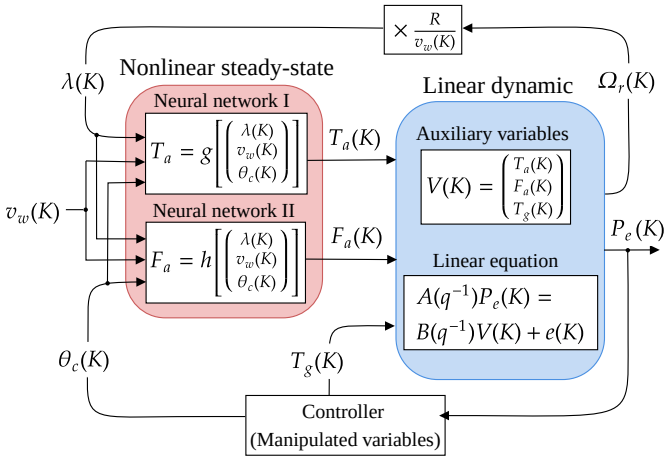


Figure 2: Wind turbine cascaded Hammerstein Structure.

III. MODEL APPROXIMATION

A. Neural cascade Hammerstein model

As discussed in [40], [41], the Hammerstein structure can represent the dynamics of the wind turbine by connecting the static nonlinear mapping in series with a Linear Time-Invariant (LTI) subsystem. The nonlinear steady-state part and a linear dynamic part are defined separately. The simulated datasets for the neural approximation include the inputs of the nonlinear steady-state subsystem (wind speed, tip-speed ratio, and pitch angle), and the main outputs are the rotor torque and rotor thrust, which are given by the following equations:

$$T_a = \frac{1}{2}\rho\pi R^3 v_w^2 C_T(\lambda, \theta_c) \tag{6}$$

$$F_a = \frac{1}{2}\rho\pi R^2 v_w^2 C_F(\lambda, \theta_c) \tag{7}$$

where C_T and C_F are the torque and thrust coefficients. The cascaded structure of the Hammerstein model is depicted in Figure 2. The input signals are the vector of aerodynamic variables, and the wind speed is the measured disturbance, while the output signals of the consecutive networks $x_r(K)$ are known as the auxiliary variables in the Hammerstein model and can be defined as follows

$$x_r(K) = w_0^{2,r} + \sum_{i=1}^{k^s} w_i^{2,r}\varphi(z_i^r(K)) \tag{8}$$

where $\varphi : \mathbb{R} \to \mathbb{R}$ is the nonlinear transfer function, K the sampling instant and $z_i^r(K)$ the sum of the input signals $u(K)$ connected to the ith node $(i = 1, \ldots, k^s)$ given by

$$z_i^r(K) = w_{i,0}^{1,r} + w_{i,1}^{1,r}\theta_c(K) + w_{i,2}^{1,r}\lambda(K) + w_{i,3}^{1,r}v_w(K) \tag{9}$$

From (8) and (9), the following outputs of rotor torque and rotor thrust can be derived

$$x_r(K) = w_0^{2,r} + \sum_{i=1}^{k^s} w_i^{2,r}\varphi\begin{pmatrix} w_{i,0}^{1,r} + w_{i,1}^{1,r}\theta_c(K) \\ +w_{i,2}^{1,r}\lambda(K) + w_{i,3}^{1,r}v_w(K) \end{pmatrix} \tag{10}$$

where i is the number of nodes in each layer, r is denoting the outputs of the neural networks (rotor torque and rotor thrust), and j is indicating the input variables including pitch angle,

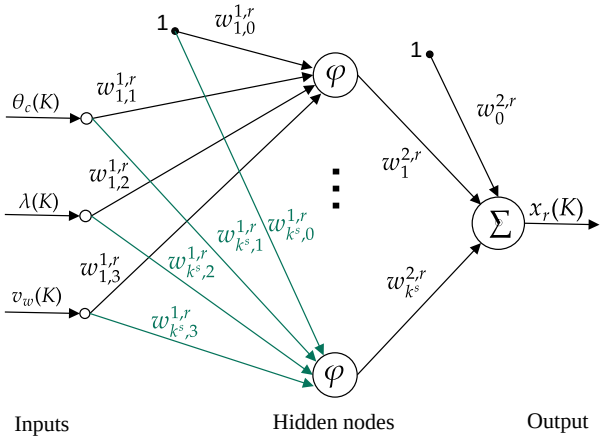


Figure 3: The neural network's structure used in the Hammerstein model

tip speed ratio, and the estimation of wind speed, which is considered as measured disturbances. Weights of the first layer and second layer are denoted by $\omega_{i,j}^{1,r}$ and $\omega_i^{2,r}$.

B. Nonlinear steady state approximation

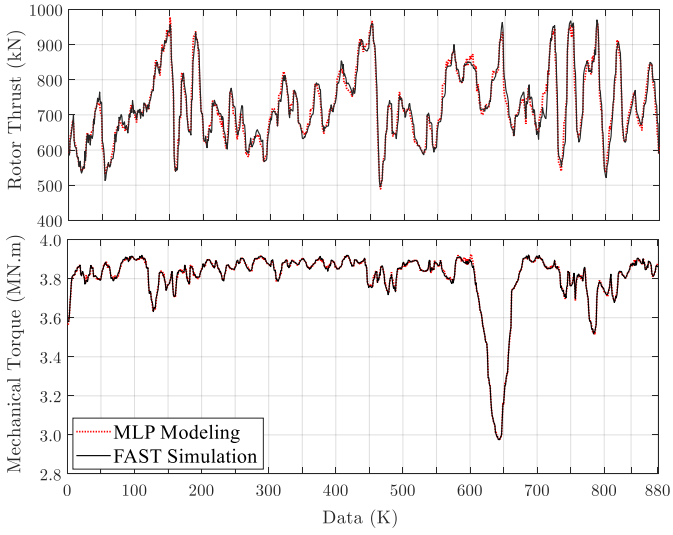
The nonlinear part is approximated by the function $g : \mathbb{R}^{n_x} \rightarrow \mathbb{R}^{n_r}$ and $h : \mathbb{R}^{n_x} \rightarrow \mathbb{R}^{n_r}$, by using the MLP neural network with $k^s = 10$ hidden nodes in the first layer and 1 node in the second layer. The neural network's structure is shown in Figure 3. The neural networks have the ability to learn the sophisticated nonlinear relationships among the inputs and accurately capture the essential aerodynamic behavior of the system in turbulent wind conditions. The datasets, including the input variables and the outputs of the nonlinear dynamic part, are obtained from simulation and randomly divided into the train, validation, and test datasets. 70% of the datasets are used to train the MLPs, and 30% of the datasets are used for test and validation. The statistical results, i.e., mean square error (MSE), error mean and error standard deviation (StD), are given in Table II. The results of the nonlinear approximation for the tested dataset are depicted in Figure 4, showing an effective and accurate performance of the MLPs.

Table II: Validation of nonlinear steady-state approximation

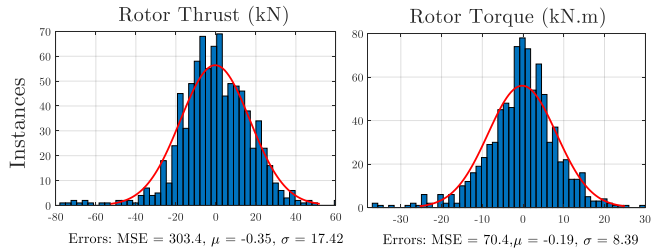
Dataset	Rotor torque (Ta)			Rotor thrust (Fa)		
	MSE	Error Mean	Error StD	MSE	Error Mean	Error StD
Train	59.6	0.04	7.72	275.08	-0.01	16.58
Validation	64.9	0.35	8.05	258.59	0.20	16.08
Test	70.4	-0.19	8.39	303.40	-0.35	17.42
All	62.0	0.05	7.87	276.86	-0.03	16.64

C. Linear approximation

The LTI subsystem must include the aerodynamics of the drivetrain, the generator, and the rotor dynamics. Therefore, the inputs of the linear dynamic part consist of the rotor thrust, the rotor torque, and generator torque, while the



(a)



(b)

Figure 4: (a) Nonlinear steady-state approximation using MLP, (b) Histogram errors of the nonlinear approximations.

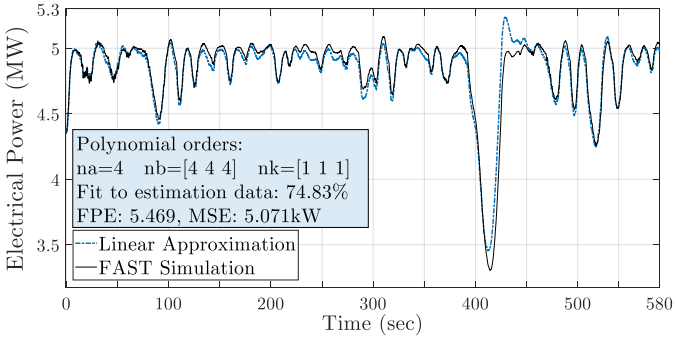


Figure 5: Linear estimation using linear ARX.

electrical power is considered as the output. A linear data-based approximation approach is proposed, based on a low-order linear ARX model, which involves the detection of the system structure by finding the regressors that have the highest contribution to the output. Figure 5 illustrates the result of the linear estimation using ARX with the fourth-order polynomial function, including the mean-square error (MSE) and the final prediction error (FPE). The auxiliary variables and the equation of the linear dynamic part can be defined by (11) and (12)

$$V(K) = \begin{bmatrix} x_r(K) & T_g(K) \end{bmatrix} \tag{11}$$

$$A(q^{-1})p_e(K) = B(q^{-1})V(K - n_k) + e(K) \tag{12}$$

where the parameters of A and B consist of polynomials of the time delay operator q^{-1} defined by (13), n_a and n_b are the constants that define the order of the LTI subsystem dynamics. The delayed order n_k is the number of input samples that occur before the input affects the output, called the system's dead time. $e(K)$ is white-noise disturbance.

$$\begin{aligned} A(q^{-1}) &= 1 + a_1 q^{-1} + ... + a_{n_a} q^{-n_a} \\ B(q^{-1}) &= b_1 q^{-1} + ... + b_{n_b} q^{-n_b} \end{aligned} \tag{13}$$

From (12) and (13), the consecutive outputs of the Hammerstein model can be calculated as follows

$$P_e(K) = \sum_{r=1}^{n_r} \sum_{l=1}^{n_b} b_l(K) V(K-1) - \sum_{l=1}^{n_a} a_l(K) P_e(K-1) \tag{14}$$

The Hammerstein model's accuracy can be improved by increasing the number of hidden layers in the neural network structure. Also, by increasing the order of the polynomial function estimating the linear dynamic behavior. In this work, the model complexity is kept as simple as possible to have a good balance between accuracy and computational complexity of the numerical optimizer.

IV. PROPOSED CONTROL STRATEGY

A. MPC algorithm based on neural Hammerstein model

In this section, the MPC algorithm based on the neural Hammerstein model is discussed, including predicting the outputs, the definition of the cost function, and on-line linearization. The general structure of the presented algorithm to control the wind turbine energy conversion system is shown in Figure 6. The vector of decision variables is calculated at each sampling instant by using quadratic optimization. The coefficients of the linear approximation of the neural Hammerstein model are calculated numerically based on the Taylor series expansion formula and can be represented as follows:

$$\begin{aligned} a_l(K) &= a_l \\ b_l(K) &= \sum_{r=1}^{n_r} b_l \sum_{i=1}^{k^s} \omega_i^{2,r} \frac{d\varphi(z_i^r(K-l))}{dz_i^r(K-l)} \omega_{i,n}^{1,r} \end{aligned} \tag{15}$$

for all $l = 1, \ldots, n_b$ and $n = 1, \ldots, n_x$. It is noteworthy to mention that the coefficients of the linearized model $a_l(K)$ and $b_l(K)$ are depending on the current operation point. In contrast, the constants a_l and b_l denote the parameters of the linear dynamic part of the model. However, thanks to the cascaded Hammerstein structure, the linear part of the model equals the linearized model's parameter at the current operating point for sampling instant K. More details can be found in [33]. Therefore, the predicted output trajectory ($p = 1, \ldots, N$ with prediction horizon N) can be calculated as follows:

$$\begin{aligned} &p_e^0(K+p|K) = \\ &\sum_{r=1}^{n_r} \sum_{l=1}^{n_b} b_l \left(w_0^{2,r} + \sum_{i=1}^{k^s} w_i^{2,r} \varphi \left(\begin{array}{l} w_{i,0}^{1,r} + w_{i,1}^{1,r} \theta_c(K-1) \\ + w_{i,2}^{1,r} \lambda_g(K-1) \\ + w_{i,3}^{1,r} v_w(K-l+p|K) \end{array} \right) \right) \\ &+ \sum_{l=1}^{n_b} b_l \left(T_g(K-1) \right) - \sum_{l=1}^{n_a} a_l P_e^0(K-l+p|K) \end{aligned} \tag{16}$$

Equation (16) can be obtained from (11), which defines the vector of axillary variables, and (14). The predicted electrical power is given by (17), which consists of two parts; the first part is a function of the currently calculated control action of pitch and torque, whereas the second part, given by (16), depends on the past measurements of manipulated variables and tip speed ratio.

$$\hat{P}_e(K) = G(K) \Delta u(K) + P_e^0(K) \tag{17}$$

where $\Delta u(K)$ is the vector of manipulated variables and is given by:

$$\Delta u(K) = \begin{bmatrix} \Delta\theta_c(K|K) \\ \cdots \\ \Delta\theta_c(K+N_u-1|K) \\ \Delta T_g(K|K) \\ \cdots \\ \Delta T_g(K+N_u-1|K) \end{bmatrix} \tag{18}$$

The dynamic matrix $G(K)$ is of dimensionality $N \times n_u N_u$ (N_u and n_u are the preset control horizon and the number of manipulated variables) consists of the step response coefficients of the linear part of the Hammerstein model, which is computed for each operating point.

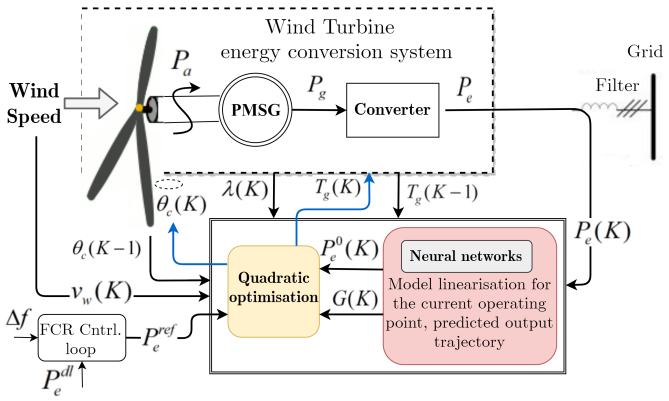


Figure 6: The structure of the MPC algorithm with nonlinear prediction and linearization for current operating point.

B. Cost function and Constraints

As mentioned in section II-B, an available power reserve is needed to be able to provide FCR. As illustrated in Figure 7, the generated output power needs to be curtailed to enable the wind turbine to provide an adequate amount of FCR in response to frequency deviations. A corresponding change in active power output is directly proportional to Δf, which is the difference between the nominal frequency $f_{\text{ref}} = 50\ Hz$ and the real-time frequency f_{actual}, with a droop coefficient of D. The relationship between active power changes and grid frequency deviations can be expressed as follows:

$$\Delta P = -D \Delta f \tag{19}$$

where Δf is the incremental change in frequency and ΔP is the incremental change in power [42]. The operating power reference P_e^{ref} of the deloaded wind turbine is calculated by:

$$P_e^{\text{ref}} = P_e^{\text{dl}} + \Delta P \tag{20}$$

The aim is to operate the wind turbine in a suboptimal mode through the deloaded control so that a certain amount of reserve is always available to supply additional active power in case of frequency deviations in a way that the droop response will adjust the reference power.

Finally, the general MPC optimization task can be defined as the quadratic optimization problem given by (21). The first term of the cost function $J(K)$ drives the electrical output towards the desired power reference, and the second term seeks to minimize variations of the control inputs.

$$\min_{\substack{\Delta u(K) \\ \varepsilon^{\min}(k),\varepsilon^{\max}(k)}} \quad J(K)$$
$$J(K) = \left\{ \begin{array}{l} \left\| P_e^{\text{ref}}(k) - G(K)\Delta u(K) - P_e^0(K) \right\|_M^2 \\ + \|\Delta u(K)\|_R^2 \\ + \rho^{\min} \left\| \varepsilon^{\min}(k) \right\|^2 + \rho^{\max} \|\varepsilon^{\max}(k)\|^2 \end{array} \right\} \tag{21}$$

subject to

$$\begin{array}{l} \theta_c^{\min} \le \theta_c(K) \le \theta_c^{\max} \\ -\Delta\theta_c^{\max} \le \Delta\theta_c(K) \le \Delta\theta_c^{\max} \\ 0 \le T_g(K) \le {T_g}^{\max} \\ -\Delta {T_g}^{\max} \le \Delta T_g(K) \le \Delta {T_g}^{\max} \\ P_e^{\min} - \varepsilon^{\min}(k) \le \hat{P}_e(K) \le P_e^{\max} + \varepsilon^{\max}(k) \\ \varepsilon^{\min}(k) \ge 0, \varepsilon^{\max}(k) \ge 0 \end{array} \tag{22}$$

where $\theta_c^{\min}$, $\theta_c^{\max}$, $\Delta\theta_c^{\max}$, ${T_g}^{\min}$, ${T_g}^{\max}$,and $\Delta {T_g}^{\max}$ are the constraints imposed on the magnitude and the increments of the blade collective pitch angle and the generator torque respectively. In the optimization problem, to avoid the feasible set to become empty, the hard output constraints can be violated by the factors ($\varepsilon^{\min}(k)$, $\varepsilon^{\max}(k)$), which determine the degree of constraint violation for the consecutive sampling instant over the prediction horizon and $\rho^{\min}$, $\rho^{\max} \ge 0$ are penalty coefficients. The diagonal matrices M and R are constantly and independently considered for the whole prediction and control horizons. The control parameters and the imposed constraints on the manipulated variables are given in Table III.

Table III: Control parameters and constraints

Parameters	Values	Definitions
$\theta_c^{\max}$	90º	Maximum blade pitch
$\theta_c^{\min}$	0º	Minimum blade pitch
$\Delta\theta_c^{\max}$	8 º/s	Maximum blade pitch rate
$\Delta\theta_c^{\min}$	-8 º/s	Minimum pitch rate
${T_g}^{\max}$	4,704 kNm	Rated generator torque
$\Delta {T_g}^{\max}$	150 kNm/s	Maximum generator torque rate
$\Delta {T_g}^{\min}$	-150 kNm/s	Minimum generator torque rate
N	10 s	Prediction horizon
N_u	3 s	Control horizon
M	1.48	Weighting factor
R	1.13	Weighting factor

The stability of the proposed MPC for wind turbine active power control can be analyzed in terms of practical stability. A very detailed analysis of the quadratic MPC with a discrete-time system can be found in [43] based on the definitions of the positively invariant set and the practical-Lyapunov function. Another very detailed analysis regarding the application issues of MPC control for Hammerstein systems is presented in [44]. A short review of MPC algorithms' stability and robustness with nonlinear models, including the specific structure of the Hammerstein model, is given in [33]. It has been discussed that the stability of the proposed MPC degrades into the feasibility of the cost function optimization process, i.e., whether a solution to the optimization problem exists or not. For stability, it is only required to calculate a feasible solution, which satisfies all the optimization problem constraints in (21). Hence, it is not essential to find the global or even a local minimum of the optimization problem at each sampling instant. Alternatively, the calculated value of the cost-function necessitates being decreasing in consecutive iterations. Although this may result in a suboptimal solution and may not lead to ideal control performance, it will guarantee the close loop stability on account of choosing the finite set control principles, and that can be a great advantage of the proposed strategy.

Moreover, to prevent excessive computation time, the repetitions are set to last for a fixed number of iterations. The execution of the MPC algorithm, running on an Intel(R) Core(TM) i7-7820 2.9 GHz CPU with 8 Gb RAM, takes less than 120 milliseconds for the maximum number of iterations ensuring smaller computational time at each time step with respect to the sampling time.

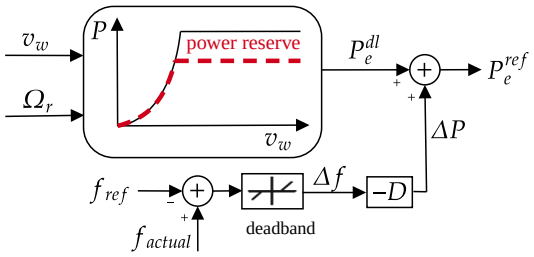


Figure 7: FCR control loop.

V. VERIFICATION AND RESULTS

In this section, we compare the results of the two control systems that have been developed to achieve the active power control of the wind turbine, which is providing FCR. Their capability of tracking the desired power reference command by actuating the generator torque and the collective blade

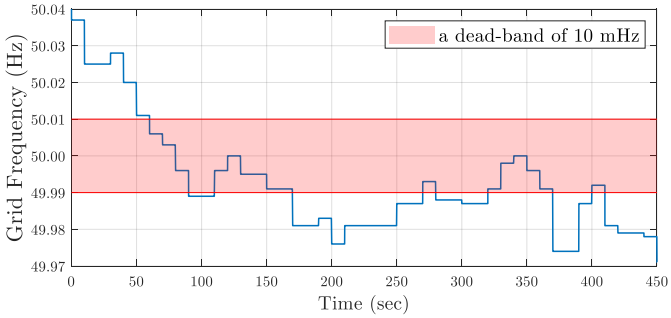


Figure 8: Frequency deviation for 450 seconds provided by ELIA (the Belgian transmission system operator).

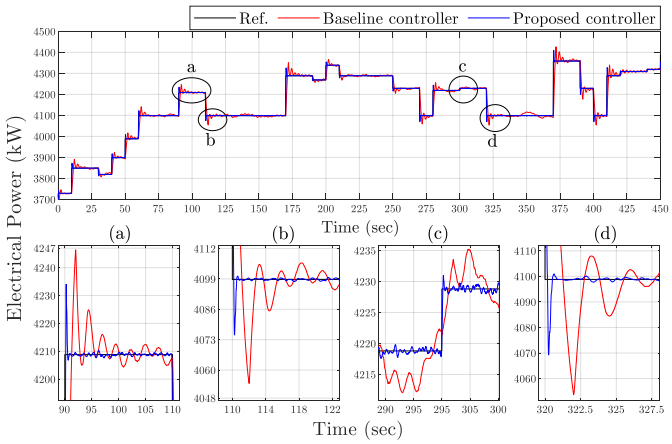


Figure 9: Wind turbine output power providing FCR.

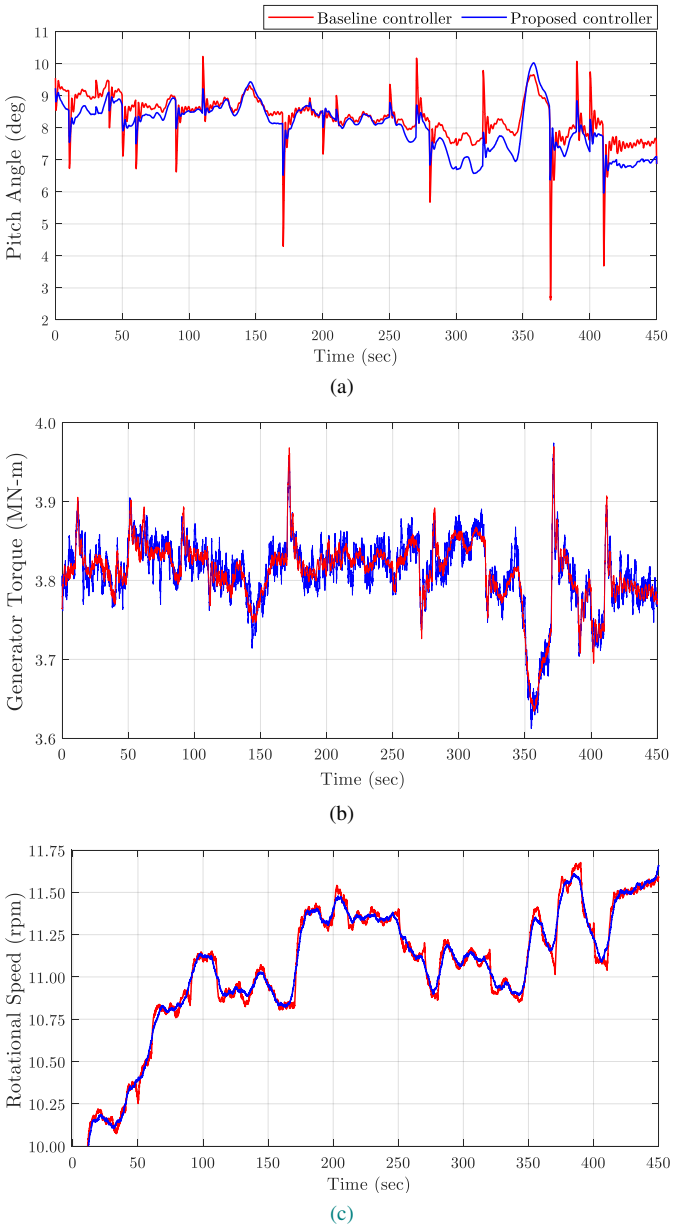


Figure 10: The performance of two control strategies for a wind speed of 15.3 with 10% TI m/s (a) Optimal behavior of pitch, (b) Generator torque reaction, (c) Rotational speed.

pitch angles is tested. Belgian TSO calculates the moving average of 10 seconds to examine whether at least 90% of the requested FCR volume is successfully delivered. In this study, a frequency profile from [45], as shown in Figure 8 with 450 seconds of the grid frequency and 10 seconds time interval, is used to test the proposed design's effectiveness in power reference tracking. Moreover, the GMDH is used to have a ten-second forecast of wind speed. Therefore, with the knowledge of the plant's dynamics, the prediction horizon is set to 10 seconds such that the dynamic model gives a good estimation. A longer prediction horizon has not been considered to avoid excessive propagation of the prediction error. Furthermore, the simulations have been carried out for the control horizon set to 10 to 50% of the prediction horizon (1s, 2s, ..., 5s). A time interval of 3s is an acceptable response and does not pose an overly enormous computational burden. Moreover, the weighting coefficients are chosen to balance the manipulated variables' increments and the reference tracking performance. The weighting matrices are set to the values given in Table III to force the Hessian matrix to be positive-definite, in which the quadratic programming has a unique solution when no constraints are defined. In this article, the wind turbine's contribution has been set to 1 MW for a 200 mHz symmetric FCR with a predefined dead band of 10 mHz. The de-loaded power set point P_e^{dl} has been set to 4.1 MW. Both of the proposed and baseline controllers respond to the frequency profile shown in Figure 8. Extensive simulations are carried out with the wind turbine subject to realistic turbulent wind speed. A realization of turbulent wind speed is used, with 10.9% turbulence intensity (TI) and 15.3 m/s mean wind speed, to make sure that the wind turbine operates in the full load region.

The results of the proposed MPC design are compared with the gain scheduling PI as the baseline controller. Figure 9 illustrates the performance of both controllers in power reference tracking. The results of the proposed MPC design are compared with the gain scheduling PI as the baseline controller. Figure 9 illustrates the performance of both controllers in power reference tracking. The Root Mean Square Error (RMSE) and Standard Deviation (StD) are commonly used to evaluate the reference tracking miss-match. The RMSE and StD values of the electrical power in the baseline strategy are 678.86 and 775.12 Watt respectively, while in the proposed strategy, these values are reduced to 36.48 and 238.77 Watt respectively. One can observe that the proposed controller ensures a stable active power response compared to the gain-scheduled PI with significantly improved tracking performance. The corresponding pitch and generator torque actions together with rotational speed are given in Figure 10 a-c, respectively. Due to the ability of the proposed control strategy to utilize a wind speed estimation and predict the optimal solution, the operation of the pitch angle is minimized. Therefore, the dynamics of the pitch system decrease as well, which may positively affect the life of the pitch mechanism and decrease maintenance costs. Also, we added a penalized soft constraint to the MPC algorithm in a way that the proposed controller will not allow the electrical power to exceed 5% of the rated value. Due to the added penalized

soft constraint, the generator torque would act in an attempt to slow down the over-speeding wind turbine with varying in small perturbations. The smoother rotor speed might also offer a damping effect on the drivetrain torsional vibrations [46].

The FAST simulator is based on blade element momentum theory and includes many features such as the effects of distributed mass and stiffness of the blades and tower, dynamic wake effects and hub and blade tip losses. In this article, the wind turbine blade and bending moments have been monitored to examine the impact of the proposed control strategy on the wind turbine structural loads. As expected, due to the minimization of the pitch action, Figure 11 shows a significant reduction in the amplitude of tower bending moments and an average reduction of blade root out-of-plane moment, while no meaningful reduction can be found in the blade root in-plane bending moment. Also, the proposed control design does not give any increase in blade root edgewise and flapwise bending moments. The RMS values of the applied loads are given in Table IV. Although the structural load mitigation was not the main objective of the proposed control design, as a side outcome, a reduction of mechanical loads (compared with the baseline control scheme) can be achieved due to the optimization of the blade control action in response to grid frequency changes.

Table IV: The RMS of applied loads

RMS Value Bending Moment (MN.m)	Baseline Controller	Proposed Controller
Blade Root In-Plane	2.79	2.75
Blade Root Out-of-plane	8.10	7.34
Tower Base Fore-Aft	53.41	49.15
Tower Base Side-to-Side	5.15	2.40

The droop constant is increased up to 100% to monitor the proposed scheme's performance near the constraints. The test results are depicted in Figure 12 for a time interval of 10 seconds. The pitch and torque variability determine the optimum operating point for the MPC controller. Figure 12 shows the upper and lower limits of pitch and torque rate, rate, illustrating the wind turbine's degree of controllability. The optimization algorithm enables the proposed design to reach the torque rate limit at a faster rate than the baseline controller while optimizing the pitch rate. As shown in Figure 12, the torque rate of the MPC at 210 seconds approaches its upper limit and supports the slow dynamics of the pitch to maintain the power reference tracking with the small overshoot. The advantage of the designed MPC is that the constraint limits can be synthetically adjusted to reduce the manipulated variables' control action or improve the power reference tracking based on the physical and operational conditions. For instance, the pitch rate constraints can be more restricted to avoid extreme actions of the pitch. Although this might result in poor reference tracking, the excessive mechanical loads will be mitigated due to pitch movement minimization.

Furthermore, the proposed MPC algorithm aims to ignore the wind disturbances that appear in the form of periodic fluctuations of wind shear instead of trying to reject them, which results in less control action in pitch and optimal

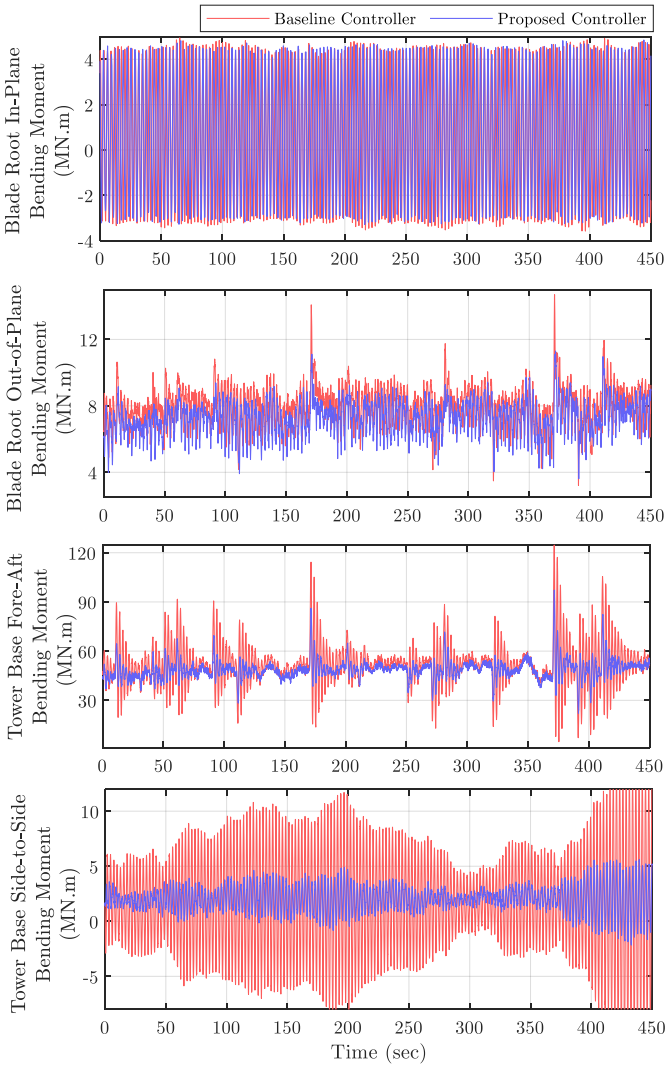


Figure 11: Wind turbine applied loads under baseline and proposed control strategies.

behavior of torque. The inflow wind speed with three different Turbulence Intensities (TI), shown in Figure 13, is applied to both controllers. The robust performance of the proposed controller against the variant TI is demonstrated in Figure 14. Another finding is that the uncertainties in wind estimation do not deteriorate the overall performance of the proposed controller, even in the presence of unexpected TI.

VI. CONCLUSION AND DISCUSSIONS

In this article, the proposed MPC enables the offshore wind turbine to provide FCR by tracking a power reference signal, given by the supplementary control loop, with an optimal pitch and torque action. The power reference tracking following a frequency disturbance has been introduced, and the robust performance of the proposed controller has been compared with the baseline controller. The proposed controller offers a stable response to frequency changes and significantly enhanced the capability of reference tracking. The stability of the control system is conducted from the system's behavior during the simulations. Moreover, the results confirm the

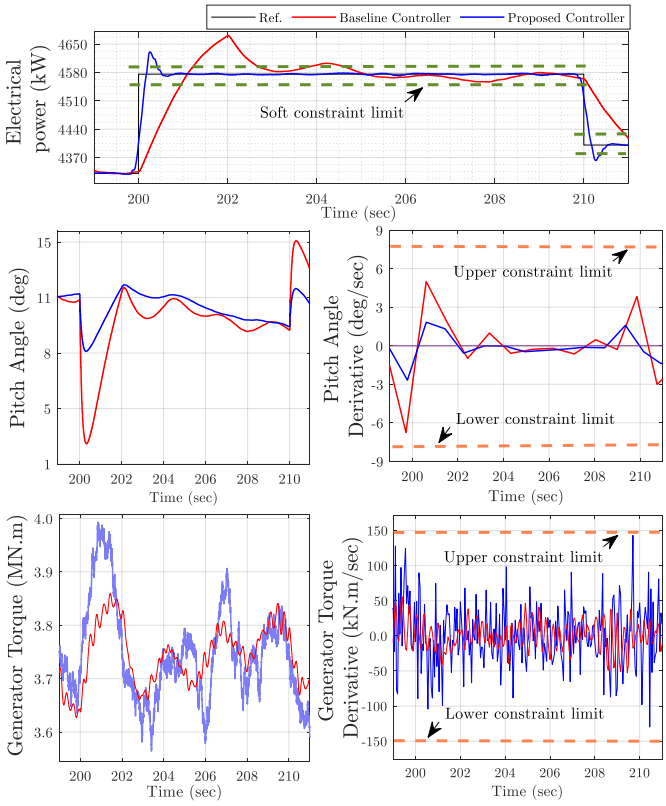


Figure 12: Operating around constraints

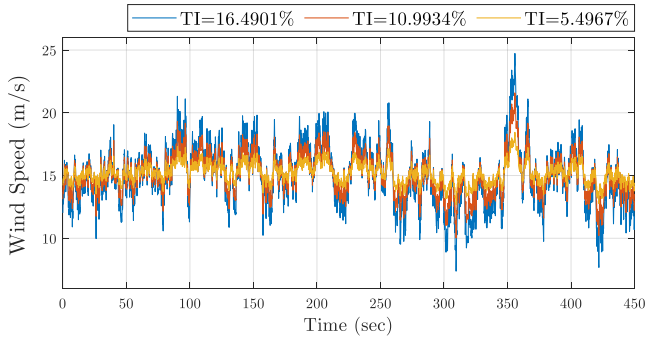


Figure 13: Wind speed with different turbulence intensities.

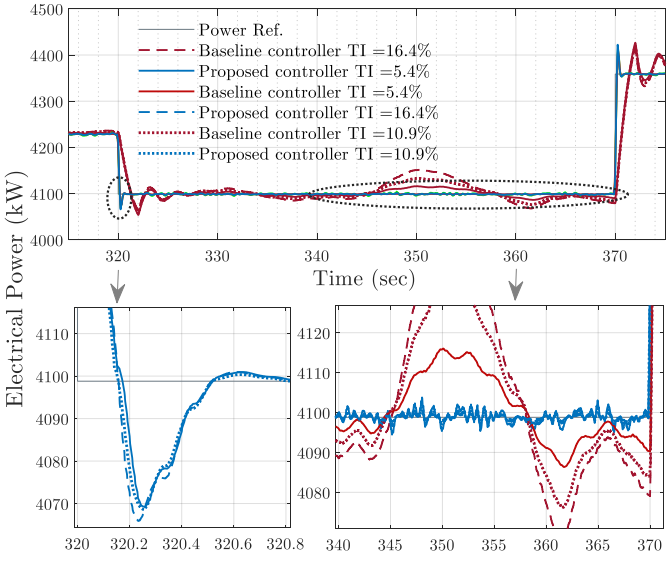


Figure 14: Robustness of the proposed controller in the presence of turbulent wind.

robust performance of the proposed controller in the presence of turbulent wind. Using the neural Hammerstein model increases the accuracy of the closed-loop system approximation. The online linearization makes it possible to use a reliable quadratic programming method and eliminates the necessity of repeating nonlinear optimization at each sampling instant. The obtained results showed that the proposed approach was able to provide FCR despite the uncertainties in terms of wind speed measurements and turbulence intensity.

Contributing to frequency regulation services may cause an increase in the blade and tower mechanical loads that leads to fatigue failures, which is an economic disincentive due to lifetime reduction. On the other hand, increasing the penetration of renewable sources has led some countries, e.g., Ireland and the UK, to set specific requirements and grid codes for wind power generating units to provide ancillary services. Therefore, employing the proposed predictive control algorithm, which is able to offer the power reserve with minimized power error and mechanical loads, can be an inspiration for many wind energy operators and encourage manufacturers for further investments.

In the future of this research, more uncertainty sets such as wind gusts and the associated controller parameters that might be corrupted with contingencies could be computed off line for the different wind speed scenarios. Therefore, an on line computational adjustment could be carried out to secure the system's behavior in all operating conditions.

ACKNOWLEDGMENT

This work was performed in the framework of the Energy Transition Fund project BEOWIND of the Belgian federal government, and the FWO research project G.0D93.16N, funded by the Research Foundation Flanders.

REFERENCES

[1] D.-A. Ciupăgeanu, G. Lăzăroiu, and L. Barelli, "Wind energy integration: Variability analysis and power system impact assessment," *Energy*, vol. 185, pp. 1183–1196, 2019.

[2] C. Edmunds, S. Martín-Martínez, J. Browell, E. Gómez-Lázaro, and S. Galloway, "On the participation of wind energy in response and reserve markets in Great Britain and Spain," *Renewable and Sustainable Energy Reviews*, vol. 115, p. 109360, 2019.

[3] V. Gevorgian, M. Singh, and E. Muljadi, "Variable frequency operations of an offshore wind power plant with hvdc-vsc," National Renewable Energy Lab.(NREL), Golden, CO (United States), Tech. Rep., 2011.

[4] S. I. Abouzeid, Y. Guo, H.-C. Zhang, and X. Ma, "Improvements in primary frequency regulation of the grid-connected variable speed wind turbine," *IET Renewable Power Generation*, vol. 13, no. 3, pp. 491–499, 2018.

[5] M. Tsili and S. Papathanassiou, "A review of grid code technical requirements for wind farms," *IET Renewable Power Generation*, vol. 3, no. 3, pp. 308–332, 2009.

[6] Z. Wu, W. Gao, T. Gao, W. Yan, H. Zhang, S. Yan, and X. Wang, "State-of-the-art review on frequency response of wind power plants in power systems," *Journal of Modern Power Systems and Clean Energy*, vol. 6, no. 1, pp. 1–16, 2018.

[7] E. Ela, V. Gevorgian, P. Fleming, Y. Zhang, M. Singh, E. Muljadi, A. Scholbrook, J. Aho, A. Buckspan, L. Pao *et al.*, "Active power controls from wind power: Bridging the gaps," National Renewable Energy Lab (NREL), Golden, CO (United States), Tech. Rep., 2014.

[8] R. M. Kamel, A. Chaouachi, and K. Nagasaka, "Three control strategies to improve the microgrid transient dynamic response during isolated mode: A comparative study," *IEEE Transactions on Industrial Electronics*, vol. 60, no. 4, pp. 1314–1322, 2012.

[9] X. Tang, M. Yin, C. Shen, Y. Xu, Z. Y. Dong, and Y. Zou, "Active power control of wind turbine generators via coordinated rotor speed and pitch angle regulation," *IEEE Transactions on Sustainable Energy*, vol. 10, no. 2, pp. 822–832, 2018.

[10] H. Wang, J. Yang, Z. Chen, W. Ge, Y. Ma, Z. Xing, and L. Yang, "Model predictive control of pmsg-based wind turbines for frequency regulation in an isolated grid," *IEEE Transactions on Industry Applications*, vol. 54, no. 4, pp. 3077–3089, 2018.

[11] S. Ghosh, S. Kamalasadan, N. Senroy, and J. Enslin, "Doubly fed induction generator (dfig)-based wind farm control framework for primary frequency and inertial response application," *IEEE Transactions on Power Systems*, vol. 31, no. 3, pp. 1861–1871, 2015.

[12] G. Xu and L. Xu, "Improved use of WT kinetic energy for system frequency support," *IET Renewable Power Generation*, vol. 11, no. 8, pp. 1094–1100, 2016.

[13] C. Luo, H. Banakar, B. Shen, and B.-T. Ooi, "Strategies to smooth wind power fluctuations of wind turbine generator," *IEEE Transactions on Energy Conversion*, vol. 22, no. 2, pp. 341–349, 2007.

[14] S. De Rijcke, P. Tielens, B. Rawn, D. Van Hertem, and J. Driesen, "Trading energy yield for frequency regulation: optimal control of kinetic energy in wind farms," *IEEE Transactions on Power Systems*, vol. 30, no. 5, pp. 2469–2478, 2014.

[15] H. Wang, Z. Chen, and Q. Jiang, "Optimal control method for wind farm to support temporary primary frequency control with minimised wind energy cost," *IET Renewable Power Generation*, vol. 9, no. 4, pp. 350–359, 2014.

[16] E. B. Muhando, T. Senjyu, A. Uehara, T. Funabashi, and C.-H. Kim, "LQG design for megawatt-class WECS with DFIG based on functional models' fidelity prerequisites," *IEEE Transactions on Energy Conversion*, vol. 24, no. 4, pp. 893–904, 2009.

[17] H. Bevrani and P. R. Daneshmand, "Fuzzy logic-based load-frequency control concerning high penetration of wind turbines," *IEEE Systems Journal*, vol. 6, no. 1, pp. 173–180, 2011.

[18] X. Yin, X. Tong, X. Zhao, and A. Karcanias, "Maximum power generation control of a hybrid wind turbine transmission system based on H∞ loop-shaping approach," *IEEE Transactions on Sustainable Energy*, vol. 11, no. 2, pp. 561–570, 2019.

[19] H. Camblong, I. Vechiu, A. Etxeberria, and M. Martinez, "Wind turbine mechanical stresses reduction and contribution to frequency regulation," *Control Engineering Practice*, vol. 30, pp. 140–149, 2014.

[20] L. Henriksen, "Model predictive control of wind turbines," Ph.D. dissertation, Technical University of Denmark, 2011.

[21] M. Mirzaei, M. Soltani, N. K. Poulsen, and H. H. Niemann, "An mpc approach to individual pitch control of wind turbines using uncertain lidar measurements," in *2013 European Control Conference (ECC)*. IEEE, 2013, pp. 490–495.

[22] M. Mirzaei, N. K. Poulsen, and H. H. Niemann, "Robust model predictive control of a nonlinear system with known scheduling variable and uncertain gain," *IFAC Proceedings Volumes*, vol. 45, no. 13, pp. 616–621, 2012.

[23] M. A. Evans, M. Cannon, and B. Kouvaritakis, "Robust mpc tower damping for variable speed wind turbines," *IEEE Transactions on Control Systems Technology*, vol. 23, no. 1, pp. 290–296, 2014.

[24] A. Kumar and K. Stol, "Scheduled model predictive control of a wind turbine," in *47th AIAA aerospace sciences meeting including the new horizons forum and aerospace exposition*, 2009, p. 481.

[25] M. Soliman, O. Malik, and D. T. Westwick, "Multiple model predictive control for wind turbines with doubly fed induction generators," *IEEE Transactions on Sustainable Energy*, vol. 2, no. 3, pp. 215–225, 2011.

[26] S. Ebadollahi and S. Saki, "Wind turbine torque oscillation reduction using soft switching multiple model predictive control based on the gap metric and kalman filter estimator," *IEEE Transactions on Industrial Electronics*, vol. 65, no. 5, pp. 3890–3898, 2017.

[30] J. Van de Vyver, J. D. M. De Kooning, B. Meersman, T. L. Vandoorn, and L. Vandevelde, "Optimization of constant power control of wind turbines to provide power reserves," in *2013 48th International Universities' Power Engineering Conference (UPEC)*. IEEE, 2013.

[27] D. Schlipf, D. J. Schlipf, and M. Kühn, "Nonlinear model predictive control of wind turbines using lidar," *Wind energy*, vol. 16, no. 7, pp. 1107–1129, 2013.

[28] D.-A. Ciupăgeanu, G. Lăzăroiu, V. Berbece, M. Tîrşu, and V. Galbură, "Modeling and control of a low power wind turbine," in *2018 International Conference on Development and Application Systems (DAS)*. IEEE, 2018, pp. 26–30.

[29] A. P. Marugán, F. P. G. Márquez, J. M. P. Perez, and D. Ruiz-Hernández, "A survey of artificial neural network in wind energy systems," *Applied energy*, vol. 228, pp. 1822–1836, 2018.

[31] J. Jonkman, S. Butterfield, W. Musial, and G. Scott, "Definition of a 5-MW reference wind turbine for offshore system development," National Renewable Energy Lab (NREL), Golden, CO (United States), Tech. Rep., 2009.

[32] J. M. Jonkman, "Dynamics modeling and loads analysis of an offshore floating wind turbine," National Renewable Energy Lab.(NREL), Golden, CO (United States), Tech. Rep., 2007.

[33] M. Ławryńczuk, *Computationally efficient model predictive control algorithms*. Springer, 2014.

[34] L. M. Tossas and S. Leonardi, "Wind turbine modeling for computational fluid dynamics," *National Renewable Energy Laboratory (NREL), Technical Report No. NREL/SR-5000-55054*, 2013.

[35] J. D. M. De Kooning, J. Van de Vyver, B. Meersman, and L. Vandevelde, "Maximum efficiency current waveforms for a pmsm including iron losses and armature reaction," *IEEE Transactions on Industry Applications*, vol. 53, no. 4, pp. 3336–3344, 2017.

[36] J. D. M. De Kooning, T. L. Vandoorn, J. Van de Vyver, B. Meersman, and L. Vandevelde, "Displacement of the maximum power point caused by losses in wind turbine systems," *Renewable Energy*, vol. 85, pp. 273–280, 2016.

[37] B. Jonkman and M. Buhl Jr, "Turbsim user's guide,National Renewable Energy Laboratory golden," CO, Technical Report NREL/TP-500-39797, Tech. Rep., 2006.

[38] A. Rettenmeier, O. Bischoff, M. Hofsäß, D. Schlipf, J. Trujillo, and M. Kühn, "Wind field analyses using a nacelle-based lidar system," in *Proc. European Wind Energy Conference*, 2010.

[39] N. Kayedpour, A. Ebneali Samani, J. D. M. De Kooning, L. Vandevelde, and G. Crevecoeur, "A data-driven approach using deep learning time series prediction for forecasting power system variables," in *IEEE 2nd International Conference on Renewable Energy and Power Engineering*, 2019.

[40] G. Van der Veen, J.-W. van Wingerden, and M. Verhaegen, "Global identification of wind turbines using a hammerstein identification method," *IEEE Transactions on Control Systems Technology*, vol. 21, no. 4, pp. 1471–1478, 2012.

[41] G. J. van der Veen, J.-W. van Wingerden, P. A. Fleming, A. K. Scholbrock, and M. Verhaegen, "Global data-driven modeling of wind turbines in the presence of turbulence," *Control Engineering Practice*, vol. 21, no. 4, pp. 441–454, 2013.

[42] Y.-Q. Bao and Y. Li, "On deloading control strategies of wind generators for system frequency regulation," *International Transactions on Electrical Energy Systems*, vol. 25, no. 4, pp. 623–635, 2015.

[43] R. P. Aguilera and D. E. Quevedo, "Stability analysis of quadratic mpc with a discrete input alphabet," *IEEE Transactions on Automatic Control*, vol. 58, no. 12, pp. 3190–3196, 2013.

[44] H. Bloemen, T. Van den Boom, and H. Verbruggen, "Model-based predictive control for hammerstein systems," in *Proceedings of the 39th IEEE Conference on Decision and Control (Cat. No. 00CH37187)*, vol. 5. IEEE, 2000, pp. 4963–4968.

[45] Elia.be, Belgian TSO providing transparency on grid data. [Online]. Available: https://www.elia.be/en/grid-data

[46] A. D. Wright and L. Fingersh, "Advanced control design for wind turbines; part i: control design, implementation, and initial tests," National Renewable Energy Lab.(NREL), Golden, CO (United States), Tech. Rep., 2008.